Journal of Colloid and Interface Science 683 (2025) 564–573

Contents lists available at ScienceDirect

Journal of Colloid And Interface Science

journal homepage: www.elsevier.com/locate/jcis

Regular Article

Free-standing bimetallic Co/Ni-MOF foams toward enhanced methane dry reforming under non-thermal plasma catalysis

Kexin Zheng [a], Xiaochun Gao [a,*], Yuhan Xie [b], Ziyang He [a], Yujiao Ma [a], Shaoqi Hou [a], Dawei Su [c,*], Xiaoguang Ma [a,*]

[a] Laboratory of Plasma and Energy Conversion, School of Physics and Optoelectronic Engineering, Ludong University, Yantai, China
[b] School of Chemistry, University of New South Wales, Sydney, NSW 2052, Australia
[c] Applied Chemistry & Environmental Science, School of Science, STEM College, RMIT University, 124 La Trobe St, Melbourne, VIC 3000, Australia

HIGHLIGHTS

- An independent BC foam supported bimetallic MOF polyhedron (Co/Ni-MOF@BC) was prepared, showing the advantage of enhancing the catalyst surface for plasma assisted DRM reaction.
- The co-coordination of Co and Ni ions in MOF polyhedrons enabled a structure uplift for the malleable BC nanofibers network with more abundant pores.
- A network structure with abundant pores is beneficial for enhancing filamentous micro discharges and surface discharges, inducing stronger plasma catalytic interactions.
- The bimetallic Co/Ni-MOF@BC exhibited a substantially improved alkaline absorption ability, favoring the more kinetically constrained CO_2 reduction.

GRAPHICAL ABSTRACT

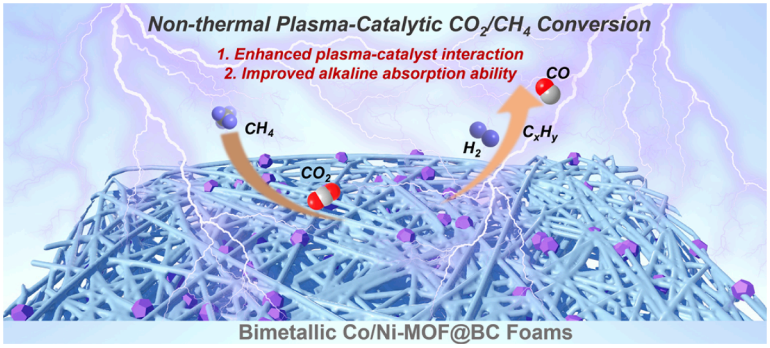

ARTICLE INFO

Keywords:
Dry methane reforming
Metal–organic frameworks
Free-standing
Filamentary microdischarge
Alkaline absorption

ABSTRACT

Understanding of the structure and interfacial merits that reactive metal–organic frameworks (MOFs) undergo is critical for constructing efficient catalysts for non-thermal plasma-assisted conversion of greenhouse gases. Herein, we proposed a free-standing bimetallic (Co/Ni) MOFs supported on bacterial cellulose (BC) foams (Co/Ni-MOF@BC) toward the coaxial dielectric barrier discharge (DBD) plasma-catalytic system, of which the Co/Ni ions coordination demonstrated an intriguing textual uplifting of the malleable BC nanofiber network with abundant pores up to micrometer-scale, which could impart a more intensive predominant filamentary microdischarge current to 180 mA with stronger plasma-catalytic interaction. Remarkably, compared to the monometallic MOF@BC foams, this bimetallic Co/Ni-MOF@BC also delivered a substantially improved alkaline absorption ability as further confirmed by the CO_2- temperature-programmed desorption (TPD) result. Benefiting from its 3D superiority and synergy of Co/Ni dual-regulation, the Co/Ni-MOF@BC, therefore, displayed the highest CO_2 and CH_4 conversion rates to 52.31 % and 71.50 %, which was above 1.5 and 1.3 times higher than those of monometallic counterparts and Co/Ni-MOF powder. Additionally, its robust cycling performance has

* Corresponding authors.
E-mail addresses: Xiaochun.Gao@ldu.edu.cn (X. Gao), dawei.su@rmit.edu.au (D. Su), hsiaoguangma@ldu.edu.cn (X. Ma).

https://doi.org/10.1016/j.jcis.2024.12.106
Received 14 November 2024; Received in revised form 14 December 2024; Accepted 15 December 2024
Available online 16 December 2024

also been evidenced by the excellent long-time DRM performance, unchanged crystallinity, morphology, and surface chemical states. By taking both the catalyst existing form and interfacial optimization of MOFs into consideration for designing a unique DRM catalyst, we believed this free-standing 3D Co/Ni-MOF@BC foams could inspire more research outputs on the design of functional catalysts with abundant pores and alkaline absorption sites to accelerate the redox kinetics of CO_2/CH_4 conversion.

1. Introduction

Over centuries, rapid industrial advancement has led to an ever-increasing demand for fossil fuels, while the massive emissions of greenhouse gas, CO_2 and CH_4, have disrupted the natural carbon balance, exacerbating global warming and other severe environmental issues [1–3]. Therefore, it has become imperative to develop new energy technologies for the utilization of greenhouse gases. Compared to the widely investigated greenhouse gas conversion techniques, including carbon capture and storage, electrochemical catalysis conversion, and microbial transformation, the reaction of dry reforming methane (DRM) that converts CO_2 and CH_4 into valuable chemical products of synthesis gas (Eq. (1)), representing a more compelling avenue for the effective utilization of waste resources in large-scale as the easy control and optimistic yield [4,5]. However, the decomposition of CO_2 and CH_4 requires a large energy input as their bond cleavage energies are relatively high at around 750 and 439.3 kJ/mol [6–9], respectively. Therefore, traditional DRM catalytic reactions are typically performed at high operating temperatures with great energy consumption, which would further lead to serious carbon deposition and catalyst deactivation, restraining the catalytic performance with both low yield and poor cycling ability [10,11].

$$CH_4 + CO_2 \rightarrow 2H_2 + 2CO,\ G_{298K} = 69\ kJ\ /\ mol \quad (1)$$

Recently, the non-thermal plasma (NTP) induced catalytic reaction has attracted increasing numerous research attention due to the mild operation condition, low cost, and high efficiency. Specifically, the plasma-excited electrons with extremely high activity are beneficial for capturing CO_2 and CH_4 molecules, thereby forming highly active substances (such as multi-excited state particles, ions, and free radicals). Although the electron temperature can reach 10^4-10^5K, the electron mass ($<10^{-30}$ kg) is extremely low [12]. Using the NTP instead of traditional catalytic thermal activation in thermal limiting reactions such as DRM can not only maintain the reaction system at around room temperature but also effectively reduce the carbon deposition or even ameliorate the catalyst deactivation caused by temperature rise [13]. Additionally, catalysts that were typically sieved or deposited on the supporting matrix in the space of a dielectric barrier discharge (DBD) reactor have been demonstrated to exhibit a synergistic conversion effect with plasma, further boosting the yield and energy efficiency of the desired products [14,15]. For example, Lin et al. loaded the NiO nanoparticles onto the γ-Al_2O_3 matrix and found a significant increase of CO_2 and CH_4 conversion rates to 80.3 % and 86.4 %, far more exceeding the plasma counterpart at around 18.3 % and 24.6 % [16]. Vakili and his colleagues also sprinkled UiO-67 on quartz cotton fibers and claimed higher CO_2 and CH_4 conversion, which was enhanced by 10 % and 18 % compared to the pure plasma experiment [17]. It is worth mentioning that powder catalysts are generally filled in the DBD reactor on the supporting matrix, such as γ-Al_2O_3, glass seeds, zeolites, quartz wools, or sieved into different meshes under high pressure [18,19]. However, these traditional catalyst loading methods have been demonstrated to display inferior catalytic activity mainly due to the compact loading density, insufficient exposed active sites, or uneven catalyst distribution [20–24], which would result in the suppression of filamentary microdischarge but dominating the surface discharge mode, further lowering the energy of electrons and radicals. Considering the catalytic reactions rely heavily on the interfacial surface properties of the core catalysts [25–27], it is therefore very reasonable to consider a better interfacial catalyst loading approach to maximize the number of exposed active sites and enhance the microdischarge effect, giving rise to overall DRM performance.

Interestingly, designing a three-dimensional (3D) framework as the supporting matrix to distribute porous catalysts has been a promising solution to optimize the interfacial surface merits of catalysts for DRM. Wang et al. used SiO_2 particles ranging from 10 to 2000 nm as templates to compare the catalytic performance of three-dimensional porous materials such as Cu and CuO with different pore sizes in NTP catalytic DRM [28]. They found that Cu-10 and CuO-1000 still exhibited higher conversion rates than empty tubes when the catalyst was completely filled. This indicates that the conversion rate in DRM reaction can still be improved as long as the catalyst structure is appropriate. In addition, Li et al. designed a 3D layered double hydroxide nanosheet supported by nickel foam (NF) with a large surface area and abundant alkaline absorption site that enabled high CH_4/CO_2 conversion rates of 16 %/9% [29]. Siliceous mesoporous foams supported by CuZnO catalyst also delivered an outstanding CO_2 hydrogenation reduction performance due to the porous structure with excellent plasma discharging behavior and radical diffusion capacity [30]. Recently, metal–organic frameworks (MOFs) have attracted extensive research attention for various plasma-catalytic applications [31,32], especially CO_2 hydrogenation and pollutant removal due to their promising gas adsorption capacity [33–35]. Inspired by this, Vakili's group performed a pioneered work employing the UiO-67 MOF as the core catalyst for DRM and discovered a combination of filamentary microdischarges and surface discharges was enhanced, thus improving the conversion of CH_4 and CO_2 by about 18 % and 10 %, respectively [17]. However, the research of tuning the MOFs nanostructure and surface property to optimize the microdischarge and alkaline absorption ability for DRM activity is still in its infant stage, and this has motivated us to carry out the current study to gain more insights.

Herein, the free-standing 3D bacterial cellulose (BC) foams supported the bimetallic-MOF polyhedrons (Co/Ni-MOF@BC) were successfully fabricated via a simple self-assembly toward the plasma-assisted DRM. Ingeniously, the co-coordination of Co and Ni ions during the MOF formation process significantly altered its nanostructure into the polyhedrons with a size of 500 nm to microns, which coincidently fitted the pores in BC to uplift the malleable cellulose nanofibers network, giving rise to more abundant pores of Co/Ni-MOF@BC foams. This textural optimization of Co/Ni-MOF@BC could induce a stronger plasma-catalysis interaction via an enhanced combination of primarily filamentary microdischarge and surface discharge mode, which rendered higher CO_2 and CH_4 conversion rates to 52.31 % and 71.50 %, far more exceeding those of monometallic Co/MOF@BC and Ni/MOF@BC. Besides, according to characterization results of CO_2-temperature-programmed desorption (TPD) curves, the bimetallic Co/Ni-MOF@BC exhibited a substantially improved alkaline absorption ability, favoring the more kinetically constrained CO_2 reduction. As a result, it displayed the highest CO yield and selectivity of 43.04 % and 69.52 %, which was 1.8 and 1.3 times higher than plasma-only and Co/Ni-MOF powder, respectively. In addition, the stability of Co/Ni-MOF@BC was evidenced to be robust with almost unchanged DRM performance, crystallinity, and morphology, as well as the surface chemical states. In summary, we have proposed a unique free-standing 3D Co/Ni-MOF@BC catalyst with both excellent structure and surface merits, which is believed to inspire more research outputs on the construction of functional catalysts with abundant pores and alkaline absorption sites to

accelerate the redox kinetics of CO_2/CH_4 conversion.

2. Experimental Section

2.1. Chemicals

Cobalt nitrate hexahydrate ($Co(NO_3)_2{\cdot}6H_2O$, 99 %, Shanghai Aladdin Biochemical Technology Co., Ltd.), nickel nitrate hexahydrate ($Ni(NO_3)_2{\cdot}6H_2O$, 99 %, Tianjin Damao Chemical Reagent Co., Ltd.), and 2-methylimidazole (2-MeIm, 99 %, Shanghai Macklin Biochemical Technology Co., Ltd.) were obtained as analytical grade chemicals without further purification. The bacterial cellulose (BC) membrane was purchased from Guilin Qihong Technology Co., Ltd.

2.2. *Synthesis of free-standing Co/Ni-MOF@BC*

The free-standing Co/Ni-MOF@BC foams were synthesized by the precipitation of MOF onto the 3D BC foams via the electrostatic interaction between the negatively charged BC and positively charged metal ions. Firstly, several BC membrane slices (4 cm × 2 cm) were immersed in 500 mL NaOH (0.01 M) solution under vigorous stirring for 5 h followed by a complete washing with deionized water until neutral. Afterwards, the pretreated BC slices were transferred into a 40 mL aqueous solution containing 388 mg $Co(NO_3)_2{\cdot}6H_2O$ and 194 mg $Ni(NO_3)_2{\cdot}6H_2O$, and kept static for 6 h to achieve adsorption equilibrium. Then these BC slices were picked into 40 mL deionized water and mixed with another 60 mL aqueous solution containing 1.64 g 2-methylimidazole (2-MeIm) dropwise, followed by gentle stirring for 2 h. Afterward, the mixture was kept in static for 5 h and washed multiple times to remove excess 2-MeIm, and finally freeze-dried for 24 h at −65 °C to obtain the puffy and free-standing Co/Ni-MOF@BC foams. For control experiments, Co-MOF@BC foams and Ni-MOF@BC foams were synthesized using similar procedures using $Co(NO_3)_2{\cdot}6H_2O$ only or $Ni(NO_3)_2{\cdot}6H_2O$ only. While Co/Ni-MOF powder was obtained using the same routine except for the use of BC foams for the absorption equilibrium.

2.3. Instrument setup for NTP-assisted DRM

The experimental setup used in this study is depicted in Fig. 1. The coaxial DBD reactor was a quartz tube with an inner diameter size of 18 mm, a thickness of 1 mm, and a length of 40 cm. The internal electrode was a 304 stainless steel tube with an inner diameter of 8 mm, which was connected to the high-voltage output. The discharge length and discharge gap were controlled to 8 cm and 5 mm, respectively. The ground electrode made of 304 stainless steel mesh was wrapped outside the quartz tube and connected to the external capacitor. Plasma was generated using a high-frequency AC high-voltage generator (CTP-2000 K, Suman Nanjing Co., Ltd.), and the discharge volage was also recorded by this instrument. The electrical signals were recorded using a digital oscilloscope (TBS 2000B series, Tektronix Co., Ltd.). A gas mixture of CH_4, CO_2, and Ar (10 %, 10 %, and 80 %) was controlled by a mass flow controller (MFC, Beijing Sevenstar Flow Co., Ltd.) and then purged into the DBD reactor in a flow rate of 30 mL min^{-1}. Following the reaction, the gas products were analyzed online using a gas chromatograph (GC 7900, Shanghai Tianmei Co., Ltd.) equipped with a thermal conductivity detector and a flame ionization detector. In this experiment, all packing materials were placed in a vacuum-drying oven at 40°C for 6 h before

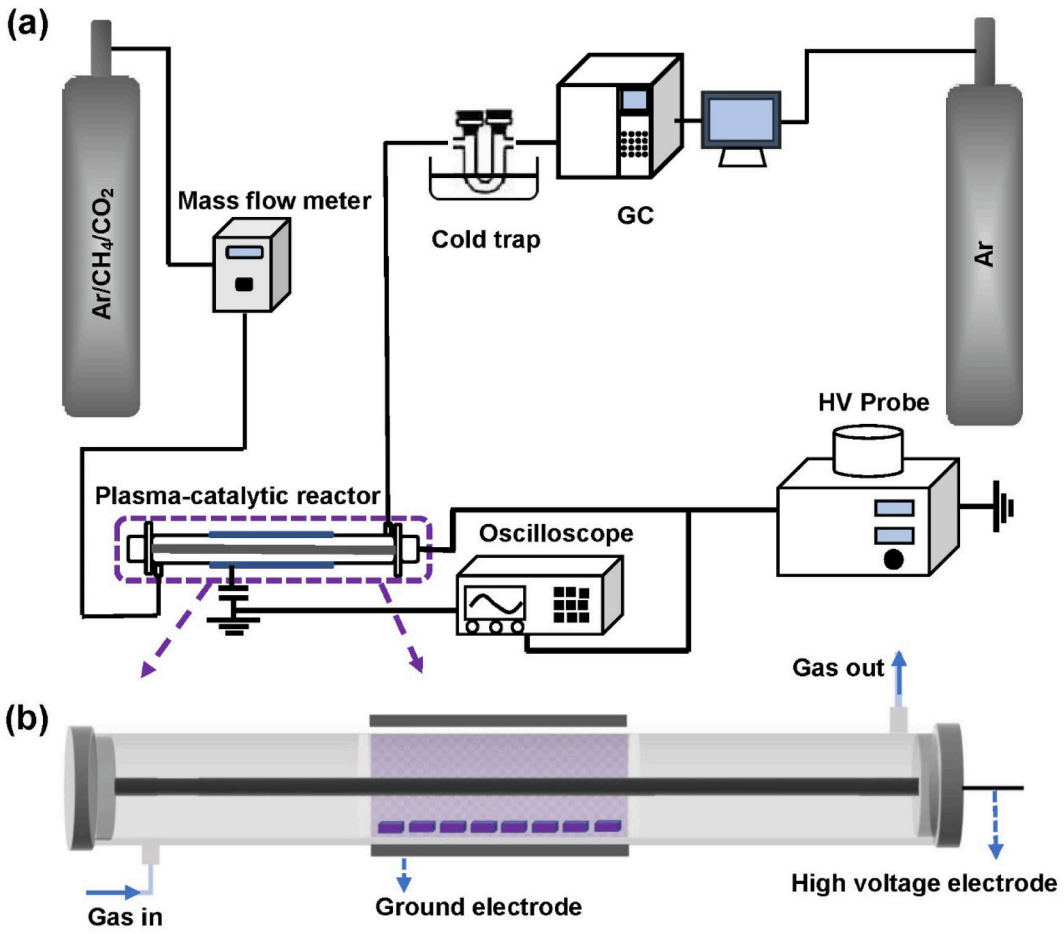

Fig. 1. Schematic diagram of **(a)** NTP setup and **(b)** enlarged DBD plasma-catalytic reactor.

being placed in the DBD reactor. Before the experiment, the packing material was subjected to the feeding gas under a discharge power of 22.5 W for 30 min, aiming to eliminate any residual traces of unreacted dimethylimidazole that might be present.

2.4. Material characterization

The morphology of the as-prepared materials was investigated using transmission electron microscopy (TEM, FEI Tecnai F20, America) and scanning electron microscopy (SEM, TESCAN MIRA LMS, America). The crystallinity of the materials was measured using an X-ray diffractometer (XRD, Rigaku D/MAX-2600, Japan). The specific surface area and pore size distribution plots were analyzed via the N_2 adsorption–desorption isotherms obtained with a Micromeritics ASAP 2460 instrument. The chemical states and surface composition of catalysts were analyzed using X-ray photoelectron spectroscopy (XPS, Thermo Scientific, America). The acidity and basicity of the materials were tested using the temperature-programmed desorption instrument (TPD, Micromeritics AutoChem II 2920, America).

2.5. Analytical methods

In this study, the reactant and product concentrations of the DRM reaction were analyzed using a gas chromatograph (GC). The following parameters were defined to evaluate the CH_4 and CO_2 conversion rates, product selectivity, product yield, and energy efficiency.

$$C_{CO_2}(\%) = \frac{CO_2 converted(mol/s)}{CO_2 input(mol/s)} \times 100 \quad (2)$$

$$C_{CH_4}(\%) = \frac{CH_4 converted(mol/s)}{CH_4 input(mol/s)} \times 100 \quad (3)$$

$$S_{CO}(\%) = \frac{CO produced(mol/s)}{CO_2 converted(mol/s) + CH_4 converted(mol/s)} \times 100 \quad (4)$$

$$S_{H_2}(\%) = \frac{H_2 produced(mol/s)}{2 \times CH_4 converted(mol/s)} \times 100 \quad (5)$$

$$S_{C_xH_y}(\%) = \frac{x \times C_xH_y produced(mol/s)}{CO_2 converted(mol/s) + CH_4 converted(mol/s)} \times 100 \quad (6)$$

$$Y_{CO}(\%) = \frac{CO produced(mol/s)}{CO_2 input(mol/s) + CH_4 input(mol/s)} \times 100 \quad (7)$$

$$Y_{H_2}(\%) = \frac{H_2 produced(mol/s)}{2 \times CH_4 input(mol/s)} \times 100 \quad (8)$$

$$Y_{C_xH_y}(\%) = \frac{x \times C_xH_y produced(mol/s)}{CO_2 input(mol/s) + CH_4 input(mol/s)} \times 100 \quad (9)$$

$$E(mol/kJ) = \frac{CO_2 converted(mol/s) + CH_4 converted(mol/s)}{Power input(kW)} \quad (10)$$

3. Results and Discussion

3.1. Nanostructure analysis

To optimize the morphology merits of 3D free-standing MOF@BC foams catalyst toward an efficient DRM reaction, we found that the metallic species were of vital importance to regulating the average size of MOFs particles. Typically, both the monometallic MOF@BC (Co-MOF@BC, Ni-MOF@BC) and bimetallic Co/Ni-MOF@BC catalysts were fabricated via facile self-assembly between metallic ions and organic ligands on the BC nanofiber foams. The abundant hydrophilic –OH groups on the BC scaffold enabled sufficient adsorption of metal ions through the electrostatic interaction, and thus, a stable metal–organic framework could be attached intimately to the substrate once dimethylimidazole was added (Fig. 2**a**, see Supporting Information, **Fig. S1**). After the freeze-drying process, the 3D Co/Ni-MOF@BC foams with both good mechanical and excellent flexible properties were obtained. As shown in Fig. 2**b**, the BC foams exhibited a morphology of a connected nanofiber network with pores ranging from tens to hundreds of nanometers and a fiber thickness of around 30 nm. Since the MOFs nanoparticles were first nucleated on the flexible BC fibers, their further growth could either enlarge the BC nanofibers pores or refill the pore space, which would have a positive or negative effect on the final exposed active sites for DRM reaction, respectively. Intriguingly, the coexistence of Co and Ni ions at a total metal usage of 2 mmol rendered the polyhedron Co/Ni-MOF units with an average size of around 1 μm, enabling both an expansion of the flexible BC nanofibers and a creation of more abundant pores without destroying the basic BC scaffold. This was also in good accordance with the rolling surface of Co/Ni-MOF@BC in comparison with the flat morphology of pure BC foams (**Fig. S2**). In contrast, we observed an opposite tendency for Co-MOF@BC that the BC nanofibers networks were split by the overlarge size of Co-MOF reaching 8 μm, which was far more exceeding the macropores in BC and thus caused a complete exposure of Co/MOF macrospheres on the supporting matrix, failing to create more pores (Fig. 2**g**, **Fig. S3**). Additionally, the exposed pores in Ni-MOF@BC were also reduced as evidenced by the over-small size of flat Ni-MOF nanoflakes at around tens to hundreds of nanometers (Fig. 2**h**, **Fig. S4**), which was very close to that of pores in BC foams, leading to a refilling of pores. Unlike the 3D free-standing MOF@BC catalysts, the as-prepared Co/Ni-MOF powder exhibited a nanoleaf structure ranging from several hundred nanometers to ten micrometers and a thickness of 170 nm (**Fig. S5**), differing from the above-mentioned morphology. These results were also consistent with previous reports that both the metal ions species and concentrations have a significant impact on the MOFs nanostructures [36–39]. Compared with the Co/Ni-MOF powder, the free-standing merit of Co/Ni-MOF@BC foams, Co-MOF@BC foams, and Ni-MOF@BC foams would render them with random clipping into slices with different sizes to fill the coaxial space in DBD reactor, providing more active sites for DRM reaction. More importantly, the synergetic use of Co and Ni ions properly regulated the size of Co/Ni-MOF polyhedrons to fit and enlarge the BC space with more pores, which was inferred to demonstrate the most favorable role for the plasma-catalytic DRM performance.

To confirm the above-mentioned more abundant pores for the bimetallic Co/Ni-MOF@BC foams in comparison with other single metallic MOF@BC foams and Co/Ni-MOF powder samples, the N_2 adsorption/desorption isotherms were further carried out in Fig. 3**a**. Obviously, Co/Ni-MOF@BC displayed a totally different type IV isotherm with a type H1 hysteresis loop, which was the typical characteristic of mesoporous materials with the corresponding size distribution at around 5 nm as reflected by Fig. 3**b**. By contrast, for other samples, we observed a type H3 hysteresis loop in the relative pressure (P/P_0) range of 0.1 to 1.0, indicating the presence of capillary condensation and the formation of silt-shaped pores caused by aggregates of particles [40]. As shown in **Table S1**, the specific Brunauer-Emmett-Teller (BET) surface area of Co/Ni-MOF@BC reached the highest value of 230.59 $m^2\ g^{-1}$, 3 times higher than that of pure BC foams. While both the single metallic Co-MOF@BC and Ni-MOF@BC displayed a similar but slightly lower BET surface area than BC foams, indicating the MOFs units covering or refilling the space in BC with a low compound concentration. Not surprisingly, the Co/Ni-MOF powder reflected the lowest surface area of 11.60 $m^2\ g^{-1}$, which was only one-twelfth of the 3D BC foams, which might indicate its nanostructure inferiority toward DRM. We ascribed the significant discrepancy in BET surface area of the free-standing Co/Ni-MOF@BC to the proper stain force induced by the tempered size of Co/Ni-MOF units, which could not only enlarge the macropores of BC but also create more abundant mesoporous structure without damaging the basic BC supporting matrix (Fig. 3**c-d**). This result was also kept in good accordance with SEM results, and the 3D bimetallic Co/Ni-

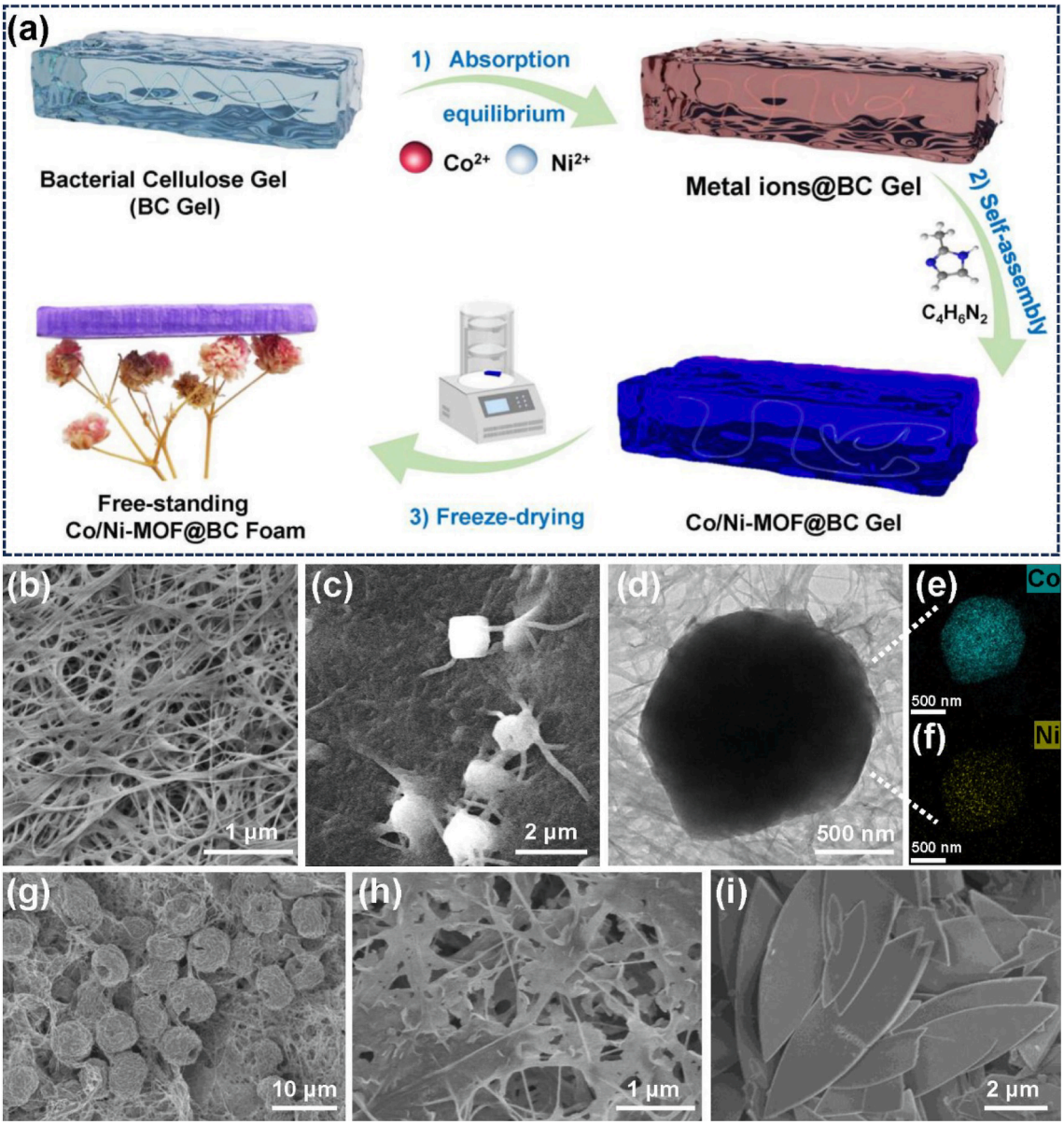

Fig. 2. **(a)** Schematic illustration of the synthetic process of the Co/Ni-MOF@BC foams; SEM images of **(b)** BC foam and **(c)** Co/Ni-MOF@BC; **(d)** TEM image of Co/Ni-MOF@BC; **(e, f)** STEM-HAADF of Co/Ni-MOF@BC; SEM images of **(g)** Co-MOF@BC foam; **(h)** Ni-MOF@BC foam; **(i)** Co/Ni-MOF powder.

MOF@BC was believed to express its synergetic effect in boosting the CO_2 and CH_4 conversion rate in terms of its morphology merits.

The core-level XPS spectra of Co and Ni elements were carried out to explore the surface chemical states discrepancy between bimetallic and monometallic MOF@BC samples (Fig. 4**a-b**). The Co 2p spectrum of Co-MOF@BC can be fitted into six peaks, of which the binding energy at around 779.4/794.9 eV and 780.9/796.6 eV were assigned to the Co^{3+} and Co^{2+} species, respectively [41] (Fig. 4**a**). Remarkably, one can observe a significant blue shift of all these peaks by 1.4 ~ 1.7 eV for the bimetallic Co/Ni-MOF@BC, which indicated the apparent change of electron distribution due to the Ni ions coordination and might have a positive effect on the CO_2 absorption. As regards the Ni 2p spectrum for Co/Ni-MOF@BC, the peaks at around 854.9/872.2 eV and 855.6/872.9 eV were identified as Ni^{2+} and Ni^{3+} species, respectively (Fig. 4**b**) [42]. However, we observed an opposite tendency in that all fitted peaks were witnessed with a red shift by 0.4 ~ 0.6 eV when compared to Ni-MOF@BC foams. The opposite directions of Co and Ni peak movements suggested an increased electron cloud density on Ni surface from Co surface, further implying the apparently mutual electronic interaction of Co and Ni ions in the bimetallic Co/Ni-MOF@BC foams. More importantly, this redistribution of electrons on transition metals was inferred to favor the CO_2 absorption or even activation as reported in other works.

It is widely acknowledged that CO_2 absorption is of vital importance for the DRM as its overhigh dissociation energy makes itself more difficult to convert than CH_4. To this end, the catalyst basicity was further evaluated by a CO_2-TPD test ranging from room temperature to 250 °C to assess the CO_2 absorption capacity for DRM. Afkhami-Ardekani et al. reported the thermal stability of ZIF-67 remained around 300 ℃ [43]. The reason for choosing this mild temperature interval was ascribed to the non-thermal plasma catalyst condition as well as the easy thermal decomposition of BC above at high temperatures. In comparison with the monometallic Co-MOF@BC foam, the bimetallic Co/Ni-MOF@BC exhibited a more positive peak position at around 124.7 and 149.5 °C and an enlarged integrated area, indicating the stronger basicity and more abundant basic absorption sites (Fig. 4**c-d**). The Ni-MOF@BC showed a similar phenomenon with lower temperature absorption peak at around 123.5 and 145.1 °C, and its integrated

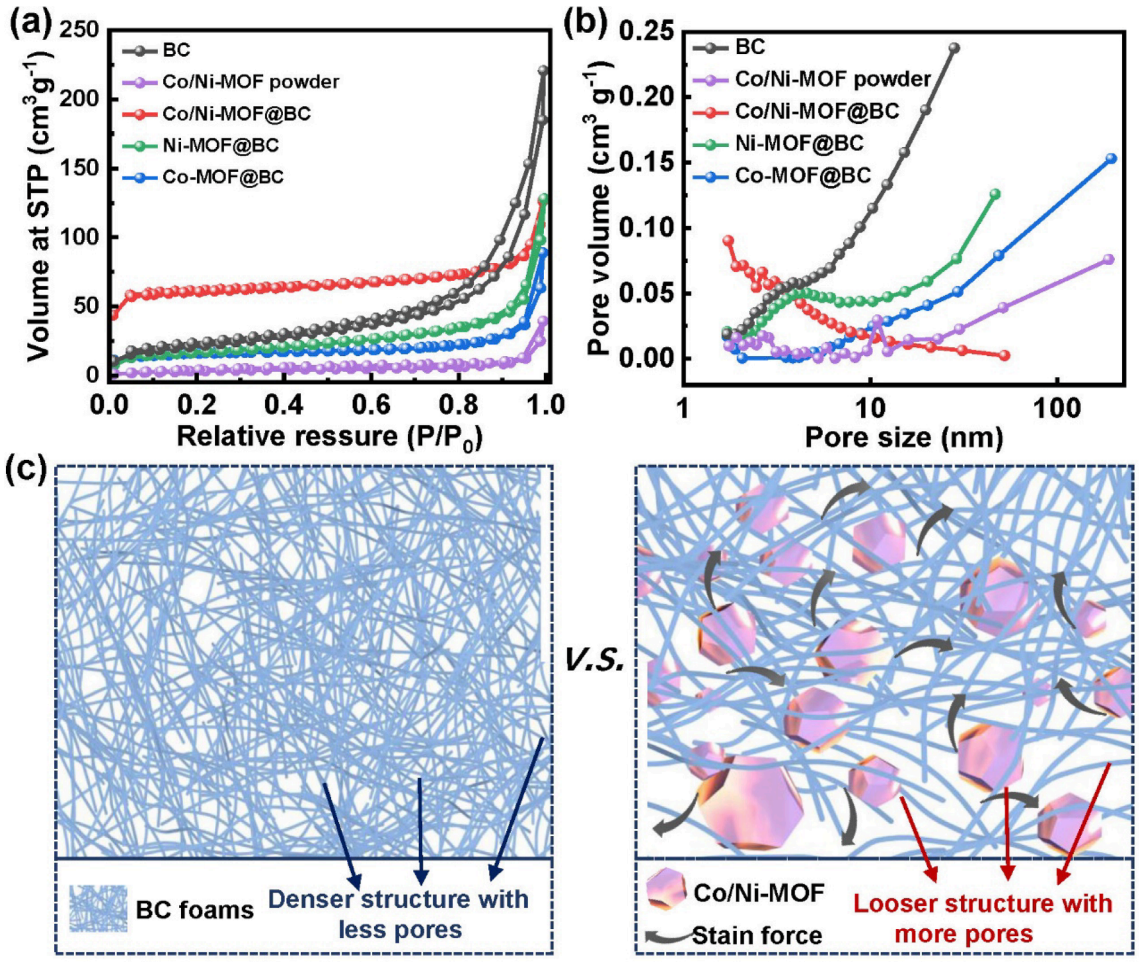

Fig. 3. **(a)** N_2 adsorption–desorption isotherms and **(b)** Pore size distributions of BC and various MOFs catalysts; **(c)** Schematic illustration of the enlarged surface area of 3D free-standing Co/Ni-MOF@BC in comparison with pure BC foams.

area was calculated to be far behind that of bimetallic Co/Ni-MOF@BC (Fig. 4**d-e**, **Table S2**), which might evidence its inferior CO_2 absorption ability among all samples. Considering the above-mentioned synergetic effect of Co and Ni metallic interaction on both structure merits and CO_2 absorption, it is thus reasonable to infer a significantly enhanced DRM catalytic performance for our bimetallic free-standing Co/Ni-MOF@BC catalyst under non-thermal plasma condition.

3.2. Catalytic performance

To study the discharge behavior of the as-prepared MOFs catalysts with different existing forms including the puffy free-standing matrix (Co/Ni-MOF@BC foams) and compact powder (Co/Ni-MOF powder), we first investigated their electronic signals in the $CH_4/CO_2/Ar$ mixture with a molar ratio of 1:1:8 under a frequency of 7.5 kHz, a fixed discharge powder of 22.5 W, and a flow rate of 30 mL min^{-1}. According to previous reports [44], the catalyst filling method has been demonstrated to have a great influence on the discharge manners, of which the partly filling method generally exhibits a superior discharge performance with both filamentary micro discharges and surface charge due to the abundant volume fraction in the gap. Herein, all samples were partly filled in the bottom of DBD reactor with a discharge length of 8 cm. As shown in Fig. 5**a**, similar to the empty tube, both the partly filled Co/Ni-MOF@BC and Co/Ni-MOF powder displayed a similar discharge mode with obvious current spikers that corresponded to the predominant filamentary microdischarge on the catalyst surface. Compared to the slightly increased current density of MOF powder than that of empty tube at around −0.08 A, the 3D free-standing Co/Ni-MOF@BC exhibited a significantly enhanced value up to 0.18 A, indicating the most substantial interaction between plasma and catalyst due to a combination of filamentous discharge mode and edge discharge mode [45,46]. Specifically, the porous Co/Ni-MOF@BC was composed of a large number of void edges, and thus, polarization electric fields were easily formed, making the local field strength higher than the average discharge field strength. Therefore, this enhanced plasma-catalysis interaction induced by our porous Co/Ni-MOF@BC foams was supposed to favor the proposed chemical reactions.

Prior to the comparable experiments, the discharge voltage was firstly optimized by evaluating the DRM performance of the empty tube under plasma-only conditions at 30, 40, and 50 kV with the $CO_2/CH_4/Ar$ molar ratio of 1:1:8 at a feeding rate of 30 mL min^{-1}, respectively. The results evidenced that with a value of 50 kV, the empty tube showed the highest CO_2/CH_4 conversion rates to 20.91 %/52.69 %, best product yields, selectivity, as well as the H_2/CO molar ratio around 1.02 (**Fig. S6**). Although the introduction of a supporting matrix reduces the discharge volume, sometimes this might lead to decreased CO_2/CH_4 conversion rates [47–50]. We observed an almost unchanged DRM performance after partly loading the BC foams at the bottom of the DBD reactor (Fig. 5**b**, **Fig. S7**), which may be attributed to the positive effect of pore microdischarge that compensated the discharge volume shrinking [28]. Based on this overall result, BC foams have demonstrated little effect on either plasma behavior or catalytic conversion, which could exclude its influence on the enhancement of DRM performance and make it comparable for various MOFs-based materials for

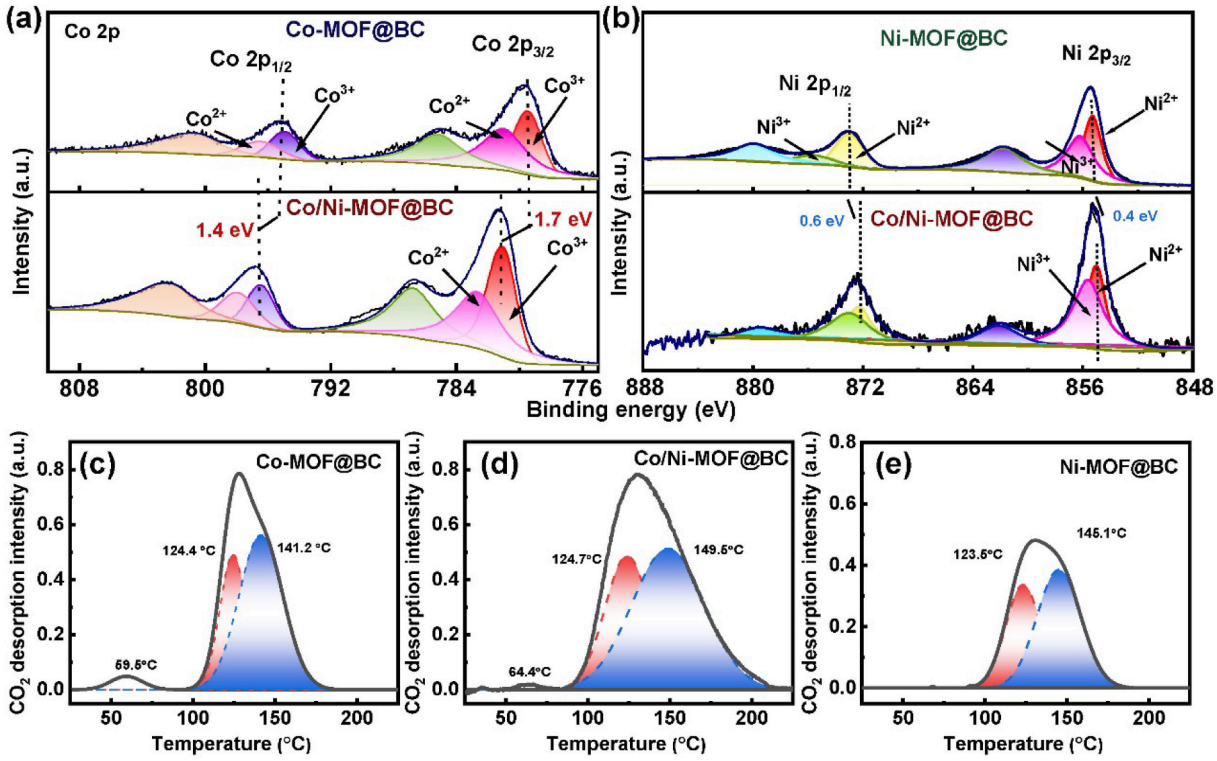

Fig. 4. Core-level XPS spectra of **(a)** Co 2p for Co-MOF@BC and Co/Ni-MOF@BC; **(b)** Ni 2p for Ni-MOF@BC and Co/Ni-MOF@BC; CO_2 -TPD profiles of **(c)** Co-MOF@BC; **(d)** Co/Ni −MOF@BC; and **(e)** Ni-MOF@BC foams.

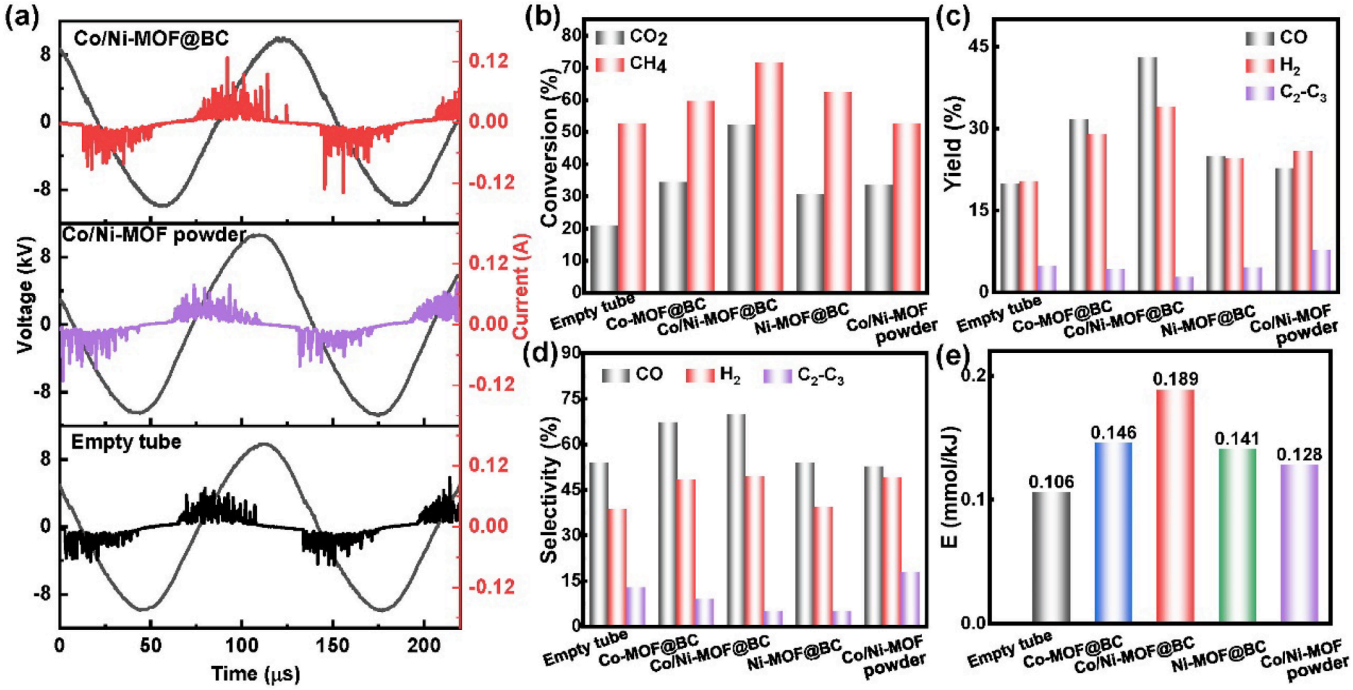

Fig. 5. **(a)** Electrical signals in a DBD plasma reactor at the frequency of 7.5 kHz and the voltage of 50 kV with different packing materials; Comparison of **(b)** CO_2 /CH_4 conversion rates; **(c)** Yields of CO, H_2, and C_2 -C_3 hydrocarbons; **(d)** Selectivity of CO, H_2 and C_2 -C_3 hydrocarbons; **(e)** Energy efficiency of empty tube and various MOFs materials at a discharge power of 22.5 W, gas feeding flow rate of 30 mL min^{-1} and CH_4 /CO_2 molar ratio of 1.

plasma-catalysis interaction evaluation.

As expected, the 3D Co/Ni-MOF@BC foams demonstrated a superior plasma-catalytic DRM performance in comparison with the monometallic MOF@BC samples and Co/Ni-MOF powder on CO_2/CH_4 conversion rates (Fig. 5**b**). Remarkably, once the monometallic MOF units were introduced onto the BC foams, the CO_2/CH_4 conversion rates of Co-MOF@BC and Ni-MOF@BC reached 34.37 %/59.58 % and 30.50 %/62.43 %, which was more than 9.59 %/9.74 % higher than plasma only condition, indicating the critical catalytic role of Co-MOF and Ni-MOF in boosting the DRM activity. Intriguingly, the bimetallic Co/Ni-

MOF@BC foams further improved the CO_2 conversion rate to 52.31 %, which was 2.5 and 1.5 times higher than the empty tube and monometallic MOF@BC foams, respectively. A similar tendency was also witnessed in the CH_4 conversion rate, among which the Co/Ni-MOF@BC ranked at the top at 71.50 %, exceeding about 18.81 % of the empty tube and BC foams. It is widely acknowledged that CO_2 dissociated energy is much larger than that of CH_4 [51], making it more challenging to construct efficient catalysts to reduce CO_2. Fortunately, according to the above-mentioned analysis, one can learn that compared to the plasma-only condition, the bimetallic Co/Ni-MOF@BC foams reflected a CH_4 conversion improvement rate by 1.36 folder while its CO_2 conversion rate exhibited a significantly sharper increase by 2.50 folder from 20.91 % to 52.31 %, evidencing its more advantageous effect in CO_2 reduction. This was mainly attributed to the more abundant alkaline absorption sites as described from the CO_2-TPD measurement (Fig. 4**c-e**). Furthermore, the bimetallic Co/Ni-MOF@BC foams also displayed a leading superiority on CO_2/CH_4 conversion over Co/Ni-MOF powder and fully packed Co/Ni-MOF@BC foams (**Fig. S8**), which confirmed the necessary for 3D nanostructure with more abundant pores and partly filling method to induce the microdischarge both outside and inside the pores to provide more energy for the breaking of molecular CO_2 and CH_4 bonds.

Correspondingly, the bimetallic Co/Ni-MOF@BC foams also reflected the highest CO and H_2 production levels at around 43.04 % and 34.02 % (Fig. 5**c**). In decreasing order, Co-MOF@BC, Ni-MOF@BC, Co/Ni-MOF powder, and empty tube displayed lower values than Co/Ni-MOF@BC, indicating the significant role of Co/Ni co-coordination and 3D textural merit. However, one can see the Co/Ni-MOF powder exhibited the highest C_2-C_3 yield at 7.85 %, which was around 2.79 and 1.66 times higher than the Co/Ni-MOF@BC and empty tube, respectively. This could be ascribed to the highest electron energy of Co/Ni-MOF@BC foams induced by the most intensive microdischarge mode, as confirmed by our electronic signals. Therefore, the hot electrons with stronger energy were more favorable in breaking the C_2-C_3 hydrocarbon bonds into shorter CO (Fig. 5**a**), rendering the highest CO but lowest hydrocarbon yield for the Co/Ni-MOF@BC sample. Accordingly, the Co/Ni-MOF@BC foams displayed the highest CO and H_2 selectivity up to 69.52 % and 47.58 %, which were close to those of Co-MOF@BC, further confirmed the superiority of bimetallic coordination of MOF units (Fig. 5**d**). Additionally, in decreasing order of the bimetallic Co/Ni-MOF@BC, monometallic Co-MOF@BC and Ni-MOF@BC, Co/Ni-MOF powder, and empty tube, the energy efficiency (E) was witnessed with a value of 0.189, 0.146, 0.141, 0.106, and 0.128, respectively (Fig. 5**e**). This tendency, the Co/Ni-MOF@BC ranking to the top, was also consistent with the above-mentioned CO_2/CH_4 conversion rate, yield, and selectivity, further indicating the best plasma-catalytic effect optimized by 3D nanostructure and superior surface chemical states.

To sum up, we ascribed this significantly improved DRM performance of bimetallic Co/Ni-MOF@BC over the monometallic MOF@BC foams to the synergetic coordination effect of Co and Ni ions, which had a profound and positive impact on the nanostructure construction with abundant pores and surface modulation with plentiful alkaline absorption sites. Firstly, the appropriate size of Co/Ni-MOF units from 500 nm to several microns enabled a strain uplift to enlarge the porous BC matrix and thus rendered with more pores, giving rise to an increased surface area and more intensive filamentary microdischarge inside or outside the pores, which would boost more active electrons to involve in the chemical reactions. Secondly, the bimetallic Co/Ni-MOF@BC also exhibited an enhanced CO_2 absorption ability according to the CO_2-TPD measurement, which was the fundamental step for highly efficient CO_2 reduction. Thirdly, the 3D free-standing BC matrix also imparted Co/Ni-MOF@BC with an overwhelming advantage role in enhancing the CO_2/CH_4 conversion rates in comparison to the compact Co/Ni-MOF powder, which further confirmed the scaffold merits of our bimetallic Co/Ni-MOF@BC foams to induce a strong plasma-catalytic interaction for DRM reaction.

Since the catalyst stability is vital for the plasma-catalytic DRM system due to the highly active electrons that might damage both the morphology scaffold and surface properties, it is essential to evaluate the corresponding long-term DRM stability, the consistency of nanostructure, and surface chemical states after reaction. It is known to all that both MOFs and BC are composed of organic co-polymers rather than robust inorganic materials such as metallic compounds, which electrons might easily attack. To this end, we first tested the long-term DRM activity of pure BC foams and Co/Ni-MOF powder to check if this would happen to our 3D free-standing Co/Ni-MOF@BC foams. As shown in **Fig. S9**, both the BC matrix and Co/Ni-MOF powder displayed stable CO_2 and CH_4 conversion rates in a 6 h plasma duration, of which the values were similar to their original values in Fig. 5**b**, revealing that the non-thermal plasma had neglectable effect on DRM activity deterioration. Notably, the bimetallic Co/Ni-MOF@BC foams also exhibited an excellent DRM performance with finally stable CO_2 and CH_4 conversion rates at around 52.5 % and 72.5 % even at 360 min, indicating the robust plasma-catalytic interaction during the reaction equilibrium (Fig. 6**a**). Furthermore, its morphology and crystallinity were also monitored by the SEM image and XRD measurement. One can see the similar nanostructure that Co/Ni-MOF units inserted into the BC nanofiber network (Fig. 6**b**) and unchanged XRD patterns when compared to the fresh Co/Ni-MOF@BC foams (Fig. 6**c**), revealing the structure stability. Besides, the core-level XPS spectra of Co 2p and Ni 2p for Co-MOF@BC remained almost the same (Fig. 6**d-e**) compared to those of the fresh sample, as described in Fig. 4**a-b**. Therefore, outstanding DRM stability has been demonstrated for 3D free-standing Co/Ni-MOF@BC foams, which might pave new insight for future researchers in designing the highly efficient DRM catalyst for large-scale applications.

4. Conclusion

In summary, we have successfully developed bimetallic-MOF polyhedrons supported on the free-standing 3D BC foams via simple self-assembly toward the plasma-assisted DRM. Ingeniously, the ingenious Co and Ni ions co-coordination rendered Co/Ni-MOF@BC foams with both a textural advantage in creating more abundant pores to induce intensive predominant filamentary microdischarge and surface merit with stronger alkaline absorption sites to boost the CO_2 absorption, respectively. Specifically, the former favored Co/Ni-MOF@BC with a 3-fold higher surface area to 230.59 $m^2\,g^{-1}$ in comparison to the BC foams due to the nanostructure uplifting of the supporting nanofibers network, which was demonstrated to deliver a significantly enhanced plasma-catalyst interaction as reflected by the highest filamentary microdischarge current to 180 mA. For the latter, the CO_2-TPD characterization results showed that Co/Ni co-regulated MOF exhibited an enhanced CO_2 absorption capacity with the highest peak area of the CO_2-TPD curve with a value of up to 45.61, which was also in good accordance with the experimental result. This would impart the bimetallic Co/Ni-MOF@BC foams with accelerated reaction kinetics for the more kinetically constrained CO_2 conversion. As a result, it displayed the highest CO_2 and CH_4 conversion rates at 52.31 % and 71.50 %, far more than those of monometallic Co-MOF@BC and Ni-MOF@BC. Along with the robust DRM catalytic stability as reflected by the consistent CO_2/CH_4 conversion rates, crystallinity, morphology, and interfacial properties after the long-time DRM evolution, we believe this unique free-standing Co/Ni-MOF@BC foams with both structural and interfacial merits would further motivate more fruitful research outputs on the precise design of a high-efficient DRM catalyst, particularly on maximizing the benefits on plasma-catalyst discharge behavior and CO_2 absorption-conversion kinetics.

CRediT authorship contribution statement

Kexin Zheng: Writing – review & editing, Writing – original draft, Visualization, Validation, Software, Methodology, Investigation, Formal

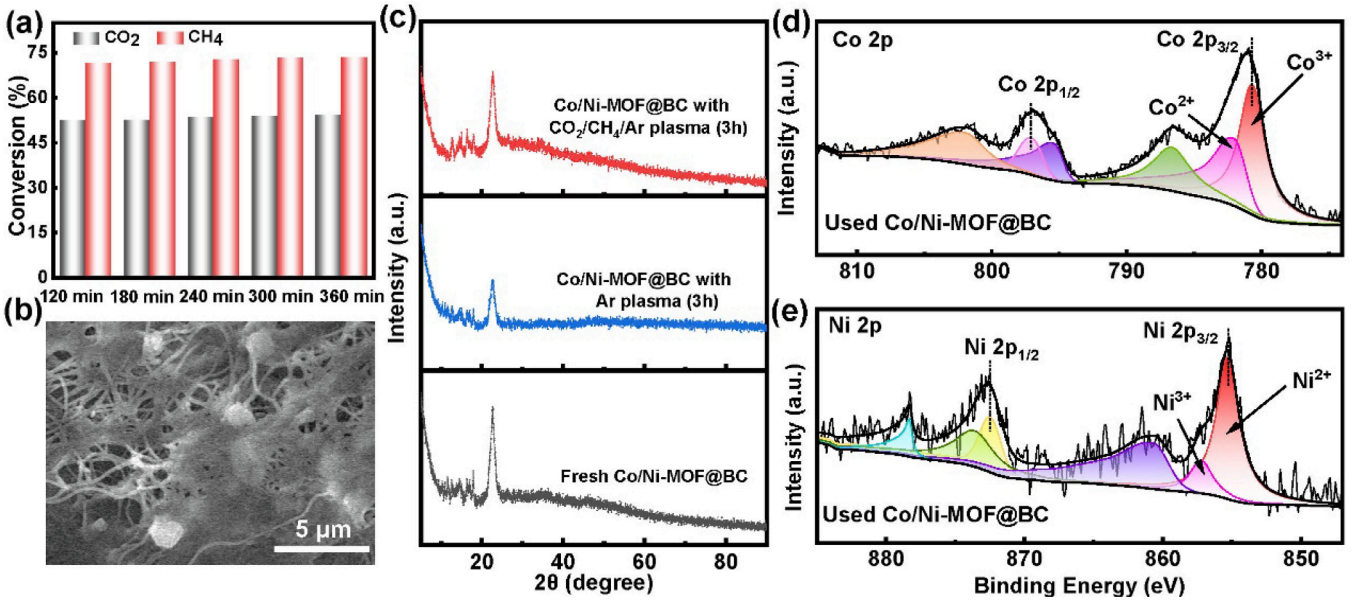

Fig. 6. **(a)** Conversion rates stability of CO_2 and CH_4 within a 6 h period of Co/Ni-MOF@BC foams at a discharge power of 22.5 W, feed flow rate of 30 mL min^{-1} and CH_4 /CO_2 /Ar molar ratio of 1:1:8; **(b)** SEM image of used Co/Ni-MOF@BC catalyst after above 6 h plasma treatment; **(c)** XRD patterns of fresh Co/Ni-MOF@BC, Co/Ni-MOF@BC after 6 h Ar-treatment and 6 h CO_2 /CH_4 /Ar-treatment; Core-level XPS spectra of **(d)** Co 2p and **(e)** Ni 2p spectra for used Co-MOF@BC foams.

analysis, Data curation, Conceptualization. **Xiaochun Gao:** Writing – review & editing, Supervision, Data curation. **Yuhan Xie:** . **Ziyang He:** Data curation. **Yujiao Ma:** Data curation. **Shaoqi Hou:** Data curation. **Dawei Su:** Supervision, Data curation. **Xiaoguang Ma:** Supervision, Project administration, Funding acquisition.

Declaration of competing interest

The authors declare that they have no known competing financial interests or personal relationships that could have appeared to influence the work reported in this paper.

Acknowledgments

This work is founded by the Natural Science Foundation of Shandong Province (ZR2022QB139, ZR2020KF025), the National Natural Science Foundation of China (12274190), and the Starting Research Fund (Grant No. 20210122) from the Ludong University. D. Su would like to acknowledge the support of the Australia Research Council (ARC) through the Discovery Project (DP230101040, DP240101548) and the Australian Renewable Energy Agency (ARENA) via the Hydrogen energy Scheme. The authors also acknowledge the support of the Carbon Neutrality Innovation Research Center at Ludong University.

Appendix A. Supplementary data

Supplementary data to this article can be found online at https://doi.org/10.1016/j.jcis.2024.12.106.

Data availability

Data will be made available on request.

References

[1] K.S. Nielsen, K.A. Nicholas, F. Creutzig, T. Dietz, P.C. Stern, The role of high-socioeconomic-status people in locking in or rapidly reducing energy-driven greenhouse gas emissions, Nat. Energy 6 (2021) 1011–1016.
[2] J. Wang, W. Azam, Natural resource scarcity, fossil fuel energy consumption, and total greenhouse gas emissions in top emitting countries, Geosci. Front. 15 (2024) 101757.
[3] H. Li, M.E. Zick, T. Trisukhon, M. Signorile, X. Liu, H. Eastmond, S. Sharma, T. L. Spreng, J. Taylor, J.W. Gittins, C. Farrow, S.A. Lim, V. Crocellà, P.J. Milner, A. C. Forse, Capturing carbon dioxide from air with charged-sorbents, Nature 630 (2024) 654–659.
[4] M. Monir Hossain, M. Robayet Ahasan, R. Wang, Influence of catalyst shape on plasma-assisted dry reforming of methane: A comparative study of Ni-CeO_2 nanocubes and nano-octahedra, Chem. Eng. J. 496 (2024) 154193.
[5] J. Slaets, B. Loenders, A. Bogaerts, Plasma-based dry reforming of CH_4: Plasma effects vs. thermal conversion, Fuel 360 (2024) 130650.
[6] C. He, Y. Gong, S. Li, J. Wu, Z. Lu, Q. Li, L. Wang, S. Wu, J. Zhang, Single-Atom Alloys Materials for CO_2 and CH_4 Catalytic Conversion, Adv. Mater. 36 (2024) 2311628.
[7] X. Meng, X. Cui, N.P. Rajan, L. Yu, D. Deng, X. Bao, Direct methane conversion under mild condition by thermo-, electro-, or photocatalysis, Chem 5 (2019) 2296–2325.
[8] J. Li, B. Huang, Q. Guo, S. Guo, Z. Peng, J. Liu, Q. Tian, Y. Yang, Q. Xu, Z. Liu, B. Liu, Van der Waals heterojunction for selective visible-light-driven photocatalytic CO_2 reduction, Appl. Catal. B 284 (2021) 119733.
[9] S. Castro, J. Albo, A. Irabien, Photoelectrochemical reactors for CO_2 utilization, ACS. Sustainable. Chem. Eng. 6 (2018) 15877–15894.
[10] A.G.S. Hussien, K. Polychronopoulou, A review on the different aspects and challenges of the dry reforming of methane (DRM) reaction, Nanomaterials 12 (2022) 3400.
[11] E. Le Saché, T.R. Reina, Analysis of Dry Reforming as direct route for gas phase CO_2 conversion. The past, the Present and Future of Catalytic DRM Technologies, Prog. Energy. Combust. Sci. 89 (2022) 100970.
[12] E.R. Cohen, B.N. Taylor, The 1986 CODATA Recommended Values of the Fundamental, Physical. Constants 17 (1988) 1795–1803.
[13] Y. Wang, W. Yang, S. Xu, S. Zhao, G. Chen, A. Weidenkaff, C. Hardacre, X. Fan, J. Huang, X. Tu, Shielding protection by mesoporous catalysts for improving plasma-catalytic ambient ammonia synthesis, J. Am. Chem. Soc. 144 (2022) 12020–12031.
[14] Y. Diao, H. Wang, B. Chen, X. Zhang, C. Shi, Modulating morphology and textural properties of Al_2O_3 for supported Ni catalysts toward plasma-assisted dry reforming of methane, Appl. Catal. B 330 (2023) 122573.
[15] Y.X. Zeng, L. Wang, C.F. Wu, J.Q. Wang, B.X. Shen, X. Tu, Low temperature reforming of biogas over K-, Mg- and Ce-promoted Ni/Al_2O_3 catalysts for the production of hydrogen rich syngas: Understanding the plasma-catalytic synergy, Appl. Catal. B 224 (2018) 469–478.
[16] S.-S. Lin, P.-R. Li, H.-B. Jiang, J.-F. Diao, Z.-N. Xu, G.-C. Guo, Plasma Promotes Dry Reforming Reaction of CH_4 and CO_2 at Room Temperature with Highly Dispersed NiO/γ-Al_2O_3 Catalyst, Catalysts 11 (2021) 1433.
[17] R. Vakili, R. Gholami, C.E. Stere, S. Chansai, H. Chen, S.M. Holmes, Y. Jiao, C. Hardacre, X. Fan, Plasma-assisted catalytic dry reforming of methane (DRM) over metal-organic frameworks (MOFs)-based catalysts, Appl. Catal. B 260 (2020) 118195.
[18] N. Bouchoul, H. Touati, E. Fourré, J.-M. Clacens, I. Batonneau-Gener, C. Batiot-Dupeyrat, Plasma-catalysis coupling for CH_4 and CO_2 conversion over mesoporous macroporous Al_2O_3: Influence of the physico-chemical properties, Appl. Catal. B 295 (2021) 120262.

[19] H.J. Gallon, X. Tu, J.C. Whitehead, Effects of Reactor Packing Materials on H_2 Production by CO_2 Reforming of CH_4 in a Dielectric Barrier Discharge, Plasma Process. Polym. 9 (2012) 90–97.
[20] H. Wang, Y. Yang, Z. Li, X. Kong, P. Martin, G. Cui, R. Wang, Plasma-assisted Ni catalysts: Toward highly-efficient dry reforming of methane at low temperature, Int. J. Hydr. Energy 48 (2023) 8921–8931.
[21] A.-J. Zhang, A.-M. Zhu, J. Guo, Y. Xu, C. Shi, Conversion of greenhouse gases into syngas via combined effects of discharge activation and catalysis, Chem. Eng. J. 156 (2010) 601–606.
[22] V. Goujard, J.-M. Tatibouët, C. Batiot-Dupeyrat, Use of a non-thermal plasma for the production of synthesis gas from biogas, Appl. Catal. A 353 (2009) 228–235.
[23] J. Sentek, K. Krawczyk, M. Młotek, M. Kalczewska, T. Kroker, T. Kolb, A. Schenk, K.-H. Gericke, K. Schmidt-Szałowski, Plasma-catalytic methane conversion with carbon dioxide in dielectric barrier discharges, Appl. Catal. B 94 (2010) 19–26.
[24] M. Kraus, B. Eliasson, U. Kogelschatz, A. Wokaun, CO_2 reforming of methane by the combination of dielectric-barrier discharges and catalysis, Phys. Chem. Chem. Phys. 3 (2001) 294–300.
[25] J. Sun, Q. Chen, W. Qin, H. Wu, B. Liu, S. Li, A. Bogaerts, Plasma-catalytic dry reforming of CH_4: Effects of plasma-generated species on the surface chemistry, Chem. Eng. J. 498 (2024) 155847.
[26] F. Polo-Garzon, Surface Reconstructions of Metal Oxides and the Consequences on Catalytic Chemistry, ACS. Catal. 9 (2019).
[27] X. Zuo, K. Chang, J. Zhao, Z. Xie, H. Tang, B. Li, Z. Chang, Bubble-template-assisted synthesis of hollow fullerene-like MoS_2 nanocages as a lithium ion battery anode material, J. Mater. Chem. A 4 (2016) 51–58.
[28] J. Wang, K. Zhang, A. Bogaerts, V. Meynen, 3D porous catalysts for Plasma-Catalytic dry reforming of Methane: How does the pore size affect the Plasma-Catalytic Performance? Chem. Eng. J. 464 (2023) 142574.
[29] J. Li, L. Dou, Y. Gao, X. Hei, F. Yu, T. Shao, Revealing the active sites of the structured Ni-based catalysts for one-step CO_2/CH_4 conversion into oxygenates by plasma-catalysis, J. CO_2 Utilization 52 (2021) 101675.
[30] Y. Chen, S. Chen, Y. Shao, C. Quan, N. Gao, X. Fan, H. Chen, Siliceous mesocellular foam supported Cu catalysts for promoting non-thermal plasma activated CO_2 hydrogenation toward methanol synthesis, Front. Chem. Sci. Eng. 18 (2024) 77.
[31] R. Pallach, J. Keupp, K. Terlinden, L. Frentzel-Beyme, M. Kloß, A. Machalica, J. Kotschy, S.K. Vasa, P.A. Chater, C. Sternemann, M.T. Wharmby, R. Linser, R. Schmid, S. Henke, Frustrated flexibility in metal-organic frameworks, Nat. Commun 12 (2021) 4097.
[32] Y. Han, G. Fan, Y. Guo, S. Guo, J. Ding, C. Han, Y. Gao, J. Zhang, X. Gu, L. Wu, Plasma-driven efficient conversion of CO_2 and H_2O into pure syngas with controllable Wide H_2/CO ratios over metal–organic frameworks featuring in situ evolved ligand defects, Angew. Chem. Int. Ed 63 (2024) e202406007.
[33] Q. Wei, S. Xue, W. Wu, S. Liu, S. Li, C. Zhang, S. Jiang, Plasma Meets MOFs: Synthesis, Modifications, and Functionalities, Chem. Rec. 23 (2023) e202200263.
[34] H. Chen, Y. Mu, Y. Shao, S. Chansai, H. Xiang, Y. Jiao, C. Hardacre, X. Fan, Nonthermal plasma (NTP) activated metal–organic frameworks (MOFs) catalyst for catalytic CO_2 hydrogenation, AIChE. J 66 (2020) e16853.
[35] F. Gorky, A. Nambo, M.L. Carreon, Cold plasma-Metal Organic Framework (MOF)-177 breathable system for atmospheric remediation, J. CO_2 Utilizat. 51 (2021) 101642.
[36] K.C. Chin, L.K. Leong, S.-Y. Lu, D.-H. Tsai, S. Sethupathi, Preparation of metal organic framework (MOF) derived bimetallic catalyst for dry reforming of methane, Ijtech 10 (2019) 1437.
[37] F. Xiang, E.J. Popczun, D.P. Hopkinson, Layer-by-layer assembly of metal-organic framework nanosheets with polymer, Nanotechnology 30 (2019) 345602.
[38] T. Kitao, Y. Zhang, S. Kitagawa, B. Wang, T. Uemura, Hybridization of MOFs and polymers, Chem. Soc. Rev. 46 (2017) 3108–3133.
[39] P.R. Yaashikaa, P. Senthil Kumar, S.J. Varjani, A. Saravanan, A review on photochemical, biochemical and electrochemical transformation of CO_2 into value-added products, J. CO_2. Utilizat. 33 (2019) 131–147.
[40] X. Ma, Y. Lou, X.-B. Chen, Z. Shi, Y. Xu, Multifunctional flexible composite aerogels constructed through in-situ growth of metal-organic framework nanoparticles on bacterial cellulose, Chem. Eng. J. 356 (2019) 227–235.
[41] C. Xu, Y. Feng, Z. Mao, Y. Zhou, L. Liu, W. Cheng, J. Wang, H. Shi, X. Liu, Binary nickel–cobalt metal–organic frameworks as electrode for high performance pseudocapacitor, J. Mater. Sci:. Mater. Electron 30 (2019) 19477–19486.
[42] X. Li, P. He, T. Wang, X. Zhang, W. Chen, Y. Li, Keggin-Type Polyoxometalate-Based ZIF-67 for Enhanced Photocatalytic Nitrogen Fixation, ChemSusChem 13 (2020) 2769–2778.
[43] M. Afkhami-Ardekani, M.R. Naimi-Jamal, S. Doaee, S. Rostamnia, Solvent-free mechanochemical preparation of metal-organic framework ZIF-67 impregnated by Pt nanoparticles for water purification, Catalysts 13 (2022) 9.
[44] X. Tu, J.C. Whitehead, Plasma-catalytic dry reforming of methane in an atmospheric dielectric barrier discharge: Understanding the synergistic effect at low temperature, Appl. Catal. B 125 (2012) 439–448.
[45] S.K. Mahammadunnisa, P. Manoj Kumar Reddy, B. Ramaraju, Ch. Subrahmanyam, Catalytic nonthermal plasma reactor for dry reforming of methane, Energy Fuels 27 (2013) 4441–4447.
[46] J.-L. Liu, X.-S. Li, X. Zhu, K. Li, C. Shi, A.-M. Zhu, Renewable and high-concentration syngas production from oxidative reforming of simulated biogas with low energy cost in a plasma shade, Chem. Eng. J. 234 (2013) 240–246.
[47] H.K. Song, J.-W. Choi, S.H. Yue, H. Lee, B.-K. Na, Synthesis gas production via dielectric barrier discharge over $Ni/\gamma\text{-}Al_2O_3$ catalyst, Catal. Today 89 (2004) 27–33.
[48] B. Eliasson, C. Liu, U. Kogelschatz, Direct conversion of methane and carbon dioxide to higher hydrocarbons using catalytic dielectric-barrier discharges with zeolites, Ind. Eng. Chem. Res. 39 (2000) 1221–1227.
[49] K. Zhang, B. Eliasson, U. Kogelschatz, Direct conversion of greenhouse gases to synthesis gas and C_4 hydrocarbons over zeolite HY promoted by a dielectric-barrier discharge, Ind. Eng. Chem. Res. 41 (2002) 1462–1468.
[50] X. Tu, H.J. Gallon, M.V. Twigg, P.A. Gorry, J.C. Whitehead, Dry reforming of methane over a Ni/Al_2O_3 catalyst in a coaxial dielectric barrier discharge reactor, J. Phys. d:. Appl. Phys. 44 (2011) 274007.
[51] A.H. Khoja, M. Tahir, N.A.S. Amin, Dry reforming of methane using different dielectric materials and DBD plasma reactor configurations, Energ. Conver. Manage. 144 (2017) 262–274.